Chapter 5   Synaptic Integration by Electro-Diffusion in Dendritic Spines

TERRENCE J. SEJNOWSKI

Computational Neurobiology Laboratory
The Salk Institute
San Diego, California

NING QIAN

Department of Brain and Cognitive Sciences
Massachusetts Institute of Technology
Cambridge, Massachusetts

I. Introduction

Many vertebrate and invertebrate neurons receive synaptic inputs on spines (Coss and Perkel, 1985). In hippocampal pyramidal cells, almost all synapses found on spines are excitatory (Harris and Stevens, 1989), but in the cat primary visual cortex, 7% of synapses on spines are inhibitory (Beaulieu and Colonnier, 1985), which comprise almost one-third of the total number of inhibitory synapses on a pyramidal cell. It has been suggested that shunting inhibition on a spine could perform a selective AND-NOT-like operation (Koch and Poggio, 1983b). The nonlinear effects would be localized to the spine, making it an effective computational module. In this chapter, we compare the predictions made by the cable model with those made by the electro-diffusion model for this problem.

The conduction of action potentials in axons can be accurately modeled by the Hodgkin–Huxley equation, which is based on the cable equation (Hodgkin and Huxley, 1952). The integration of postsynaptic signals in dendrites has also been studied with analytic solutions to passive cables (Rall, 1977), and recently, several investigators have used the cable model to examine the possibility of more complex signal processing in dendrites with complex morphologies, multiple synaptic inputs, and passive or excitable membranes (Shepherd *et al.*, 1985;

117

Koch and Poggio, 1983; Koch *et al.*, 1983; Rall and Segev, 1985; Perkel and Perkel, 1985; Wathey *et al.*, 1989). A central assumption of the cable model is that ionic concentrations do not change appreciably, so that the driving forces can be approximated by fixed batteries. However, if the intracellular volume is relatively small, as in dendritic spines, then ionic concentrations can change rapidly following a transient change in ionic conductances. Moreover, a sudden change in concentration at one location can lead to gradients of ionic concentration within a thin process, such as the neck of a spine, which violates another fundamental assumption of the cable model. Under these circumstances, it is necessary to consider the fundamental laws governing the movements of ions, as given by the Nernst–Planck equations for electro-diffusion (Jack *et al.*, 1975).

In this chapter, we summarize the results of applying an electro-diffusion model based on the Nernst–Planck equation to dendritic spines (Qian and Sejnowski, 1989, 1990). The electro-diffusion model gives more accurate predictions than the cable model, especially for small structures. The electro-diffusion model provides a unified framework for the computation of both the membrane potentials and the intracellular ionic concentrations during synaptic activation. We have also developed a modified cable model that is a better approximation to the electro-diffusion model than the standard cable model and is less demanding computationally.

II. Cable Model Predictions

Consider first the case where the excitatory and inhibitory synapses are very close to each other. According to the cable model, the excitatory and the inhibitory synaptic currents are, respectively, given by:

$$I_e(t) = G_e(t)(V(t) - E_e) \tag{1}$$

and

$$I_i(t) = G_i(t)[V(t) - E_i] \sim G_i(t)[V(t) - V_{\text{rest}}], \tag{2}$$

where E_e and E_i are the reversal potentials of the excitatory and the inhibitory synapses, G_e and G_i are the transient synaptic conductances, V is membrane potential at the synapse, and V_{rest} is the resting membrane potential (Rall, 1977).

We have assumed in Eq. (1) that the reversal potential for shunting inhibition is very close to the resting membrane potential. In contrast, the excitatory inputs usually cause conductance increases to ions like Na^+ or Ca^{++} that have a reversal potential, E_e, well above resting membrane potential. The inhibition will be effective if $|I_i|$ is comparable to $|I_e|$. This requires, first, that G_i be larger than

G_e. Second, V should be well above the resting membrane potential so that the driving force for the inhibition $(V - V_{rest})$ is comparable to the driving force for the excitation $(V - E_e)$. This in turn requires that G_e be large and/or that the synapses are on small structures, such as spines or thin dendrites, where input resistances are large and small synaptic conductance change can cause a large depolarization. (Large inhibitory driving forces can also be achieved when the cell is firing an action potential.) In summary, for shunting inhibition to be effective when excitation and inhibition are located close to each other, the cable model requires that the synapses should be on small structures and $G_i > G_e \gg G_{rest}$, where G_{rest} is resting conductance of the membrane at the synapse.

In their analysis and simulations of shunting inhibition, Koch *et al.*, (1983) mainly considered large synaptic conductances on spines and distal (thin) dendrites that satisfy the inequalities discussed in the preceding. Their G_e was as large as 10 nS and G_i was 100 nS, but more recent physiological data suggest that G_e should be about 1 nS (Higashima *et al.*, 1986; Brown *et al.*, 1988). They also found that, for large excitatory conductances, inhibition on the direct path to the cell body was also effective, and that the most effective location for the inhibition moves toward the soma as the excitatory conductance increases (Koch *et al.*, 1982). Two opposing factors explain the phenomenon: When the inhibition is on the direct path from excitation to the soma, I_i is smaller because, at the site of inhibition, the membrane is less depolarized; but I_e is also smaller because, at the site of inhibition, the membrane is less depolarized; but I_e is also smaller because, at the site of excitation, the membrane is more depolarized. They also found that when the inhibition was more distal than the excitatory synapse, the inhibition was no longer effective. In this case, the resistance from the excitatory synapse to the cell body is much less than the resistance to the inhibitory synapse at the distal tip, so less current is shunted. Finally, Koch *et al.*, (1983) mentioned that increasing the value of the cytoplasmic resistivity and the membrane resistance increased the effectiveness of inhibition. This occurred because the membrane depolarization was larger, which made the driving force for the inhibitory current larger and the driving force of the excitatory current smaller.

III. Limitations of the Cable Model

In the cable model, the membrane potential, $V(z, t)$, at distance z and time t along a cable obeys the equation (Jack *et al.*, 1975):

$$\frac{d}{4R_i} \frac{\partial^2 V}{\partial z^2} = C_m \frac{\partial V}{\partial t} + I_m, \tag{3}$$

where d is the diameter of the cable, R_i (Ωcm) is the total intracellular cytoplasmic resistivity, C_m (μF/cm^2) is the membrane capacitance per unit area, and I_m (mA/cm^2) represents the total non-capacitative membrane current density, which is the summation of all non-capacitative membrane current densities for each ionic species, $I_{m,k}$. If we assume that the movement of ionic species k across the membrane can be described by a membrane resistance of unit area $R_{m,k}$ (Ωcm^2) in series with a battery whose electromotive force E_k is equal to the ionic equilibrium potential, then

$$I_{m,k} = \frac{V - E_k}{R_{m,k}} \tag{4}$$

and

$$I_m = \sum_k I_{m,k} = \frac{V - V_{rest}}{R_m}. \tag{5}$$

where the resting membrane potential V_{rest} and the total membrane resistance R_m are given by:

$$V_{rest} = R_m \sum_k (E_k/R_{m,k}), \tag{6}$$

$$\frac{1}{R_m} = \sum_k (1/R_{m,k}). \tag{7}$$

Through these definitions, the electrical circuit can be reduced to a simpler equivalent circuit that has a single battery in series with a leak resistance. The standard equation for the cable model is obtained by substituting Eq. (5) into Eq. (3), assuming that V is measured from the resting potential V_{rest} (Rall, 1977):

$$\lambda^2 \frac{\partial^2 V}{\partial z^2} = \tau_m \frac{\partial V}{\partial t} + V, \tag{8}$$

where the space and time constants are defined as

$$\lambda = (d\,R_m/4R_i)^{1/2}, \tag{9}$$

$$\tau_m = R_m\,C_m. \tag{10}$$

The electromotive forces of the membrane batteries (equilibrium potentials) in the cable model are usually obtained from the Nernst equation and are considered constants. This is a good approximation in the squid giant axon or other large neurons, but may introduce errors if the concentrations of some ions change significantly. This applies to Ca^{++} in many situations and to synaptic events in

small structures such as dendritic spines (Rall, 1978; Koch and Poggio, 1983a; Zador *et al.*, 1990).

A second limitation of the cable model is in the treatment of longitudinal spread of current within neurons. In the cable model, the gradient of the electrical potential in the cytoplasm is the driving force for the ionic current, but there is no provision for the driving forces due to concentration gradients. This is usually a good assumption, but it may not be valid for small structures like dendritic spines where the spatial concentration gradients can be very large.

Finally, different ions may have different concentration-dependent cytoplasmic resistivities, but the cable model only incorporates the total cytoplasmic resistivity. This may not be a valid approximation when the concentration of ions are changing differentially. In summary, one expects that the cable model may not be appropriate when spatial and/or temporal ionic concentration changes are large and, especially when ionic concentration changes need to be determined.

IV.   Electro-Diffusion Model Predictions

The cable model fails for small structure and large conductance changes, precisely the conditions required for effective shunting inhibition by the cable model (Qian and Sejnowski, 1988, 1989). the electro-diffusion model predicts that the shunting inhibition cannot be effective on small structures for the following reasons. Consider first the case when the conductance changes are large. If the inhibitory current is carried by Cl^- ions, then during a large conductance change the Cl^- concentration in a small structure such as a spine or a thin dendrite will very rapidly increase. The Nernst potential for Cl^- becomes more positive and the inhibition is ineffective. Changes in the Cl^- Nernst potential have been reported (Griffith *et al.*, 1986; Huguenard and Alger, 1986). If the conductance changes are small, then the concentration changes for Cl^- are small and the electro-diffusion model will reduce to the cable model. Thus, shunting inhibition will not be effective because the membrane depolarization is small and the driving force for the inhibitory current is much smaller than that for the excitatory current, as discussed in section II. As a consequence, the electro-diffusion model predicts that the shunting inhibition can never be very effective in small structures.

A similar analysis can be applied for hyperpolarizing inhibition carried by K^+. When both the excitatory and the inhibitory synaptic conductances are large on a small structure, K^+ hyperpolarizing inhibition is just as ineffective as the Cl^- shunting inhibition because of large ionic concentration changes. However, the situation for small synaptic conductances is different. The reversal potential

for K^+ is sufficiently below the resting potential that the driving force for the inhibition can be large even at the resting potential. In addition, the intracellular K^+ concentration is much higher than Cl^- and, therefore, the percentage change is usually smaller. These statements will be made quantitatively precise in the model and the numerical simulations presented next.

A.   Electro-Diffusion Model

The movement of ions in neurons is governed by the Nernst-Planck equation (Jack *et al.*, 1975):

$$\bar{J}_k = -D_k(\bar{\nabla} n_k + (n_k/\alpha_k)\bar{\nabla} V), \tag{11}$$

where V is the potential, $\bar{J}_k$ is the flux of ionic species k (number of particles per unit area), D_k is the diffusion constant, n_k is the concentration, and the constant α_k is defined as

$$\alpha_k = \frac{RT}{Fz_k}, \tag{12}$$

where z_k is the valence of ionic species k, R is the gas constant, F is the Faraday constant, and T is the absolute temperature. The ionic concentrations and ionic currents must additionally satisfy the continuity equation:

$$\bar{\nabla} \cdot \bar{J}_k + \frac{\partial n_k}{\partial t} = 0. \tag{13}$$

Consider a cylinder of diameter d and assume that the longitudinal current and ionic concentrations are uniform across the transverse cross section of the cylinder. Assume also that transverse currents occur only at the surface of the cylinder and are independent of angle around the axis of the cylinder. These assumptions reduce the problem of electro-diffusion to a one-dimensional problem along the axis of the cylinder. The equations can be written in cylindrical coordinates and reduced to a single equation for the concentration as a function of the distance along the z axis of a cylinder:

$$\frac{\partial n_k}{\partial t} = D_k \frac{\partial^2 n_k}{\partial z^2} + \frac{D_k}{\partial_k} \frac{\partial}{\partial z}\left(n_k \frac{\partial V}{\partial z} \right) - \frac{4}{d} J_{m,k}, \tag{14}$$

where $J_{m,k}$ is the membrane flux of ionic species k, positive for outgoing flux.

Equation (14) must be supplemented by an additional constraint between the membrane potential and the ionic concentrations. We adopt the same capacitative model of the membrane used in the cable model; that is, we assume that the

potential change in a short segment of a process is equal to the change of the total charge in the segment divided by its membrane capacitance:

$$V(z, t) = V_{\text{rest}} + (Fd/4C_{\text{m}}) \sum_k [n_k(z, t) - n_{k,\text{rest}}]z_k, \tag{15}$$

where V_{rest} is the initial potential and $n_{k,\text{rest}}$ is the initial ionic concentration of species k.

Neuronal processes often branch and change their diameters. If branches are allowed, then these equations must be solved on a tree rather than a line. Continuous diameter changes can be approximated by segments having piecewise constant diameters. At points where the diameter jumps and/or branches occur, the solutions can be matched using the continuity of flux at that point. The continuity constraint at a branch point can be derived from Eq. (11). The continuity constraint at a branch point where three processes join is given by:

$$d_1^2 \left(\frac{\partial n_k}{\partial z} + \frac{n_k}{\alpha_k} \frac{\partial V}{\partial z} \right) \bigg|_1$$
$$= d_2^2 \left(\frac{\partial n_k}{\partial z} + \frac{n_k}{\alpha_k} \frac{\partial V}{\partial z} \right) \bigg|_2 + d_3^2 \left(\frac{\partial n_k}{\partial z} + \frac{n_k}{\alpha_k} \frac{\partial V}{\partial z} \right) \bigg|_3, \tag{16}$$

where d_i is the diameter of the ith branch.

The square of the diameter enters into this equation because the flux through the areas of each branch must be matched. There is an analytic solution of the cable model for branching dendrites having passive membranes if Rall's *3/2 power law* (Rall, 1977) is satisfied. This law for an equivalent cylinder does not hold for our electro-diffusion model except in the limit when the concentration gradients go to zero and Eq. (4) is used to compute the membrane currents. A compartment approximation for the solution of Eq. (14) is inaccurate for large ionic fluxes if the continuity constraint in Eq. (16) is not used to match solutions on the two sides of a diameter jump or at a branch point.

B.   *Simulations of Postsynaptic Potentials in a Dendritic Spine*

For simplicity, only three types of ions, K^+, Na^+ and Cl^-, will be considered in this chapter. Excitation was modeled by a combination of transient conductance changes to Na^+ and K^+, with the K^+ conductance equal to one-tenth of Na^+ conductance (Hille, 1984). The synaptic reversal potential under this combination is about 50 mV. We also made simulations with the reversal potential of the excitatory synapse equal to 0 mV and similar conclusions were obtained. Silent shunting inhibition and hyperpolarizing inhibition were modeled by transient Cl^-
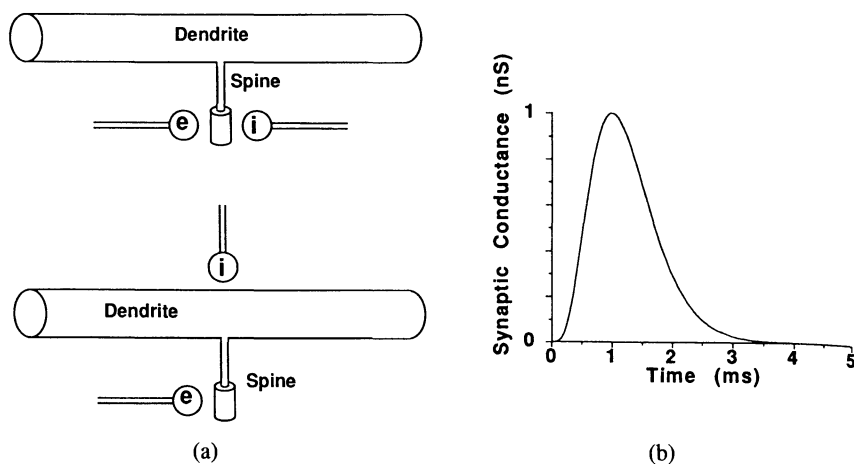
FIGURE 1.   (a) Geometry of the dendrite and spine for the simulations showing excitation and inhibition on the spine head (top) and inhibition on the dendritic shaft at the base of the spine (bottom). The spine was located in the center of a dendrite with total length 300 μm and diameter 1 μm; the spine neck was 1 μm long and 0.1 μm in diameter; the spine head was 0.69 μm long and 0.3 μm in diameter. In the simulations of the electro-diffusion model, sample points in the dendrite were 10 μm apart and the integration time step was 10^{-7} sec; in the spine head and neck, the spacing was 0.173 μm and 0.167 μm, respectively, and the time steps were 2×10^{-9} sec. The model had a total of 41 sample points: 31 in the dendrite, six in the spine neck, and four in the spine head. In the conventional cable model, only 33 lumped compartments were used (one for head, one for neck, and 31 for dendrite) due to the large spatial constant. The time step for spine head and neck was 10^{-7} sec and that for the dendrite was 10^{-6} sec. (b) Excitatory and inhibitory synaptic conductance changes were modeled by $G(t) = G_M (et/t_{peak})^4 e^{-4t/t_{peak}}$, where t_{peak} was the time to reach the peak conductance, G_M. A graph of this expression is shown with $t_{peak} = 1$ ms, and $G_M = 1$ nS. Parameters used in our simulations were: $t_{peak} = 1$ ms; membrane capacitance $C_m = 1$ μF/cm^2; diffusion coefficients $D_K = 1.96 \times 10^{-5}$ cm^2/sec, $D_{Na,M} = 1.33 \times 10^{-5}$ cm^2/sec, and $D_{Cl} = 2.03 \times 10^{-5}$ cm^2/sec; resting membrane conductances of unit area $g_{K,rest} = 1.95 \times 10^{-4}$ Scm^2, $g_{Na,rest} = 1.63 \times 10^{-5}$ Scm^2, and $g_{Cl,rest} = 3.89 \times 10^{-5}$ Scm^2; initial intracellular concentrations $n_{K,0} = 140$ mM, $n_{Na,0} = 12$ mM, and $n_{Cl,0} = 5.5$ mM; extracellular concentrations $n_{K,out} = 4$ mM, $n_{Na,out} = 145$ mM, and $n_{Cl,out} = 120$ mM. With this set of parameters, the resting membrane potential was -78 mV. The Nernst potentials for K$^+$, Na$^+$, and Cl$^-$ were -90 mV, 63 mV, and -78 mV, respectively. Total membrane resistivity R_m was 4000 Ωcm^2. Total cytoplasmic resistivity R_i at rest was calculated (Qian and Sejnowski, 1989) to be 87 Ωcm. Total surface area of the spine head was 0.65 μm^2. Some of these parameters were varied, as explained in the relevant figures or tables. The sources for these parameters are given in Qian and Sejnowski (1989).

and K^+ conductance changes, respectively. Ionic driving forces similar to Eqs. (1) and (2) were used for the electro-diffusion model rather than the constant-field approximation used in Qian and Sejnowski (1989). The Nernst Potentials were updated at each time step according to the instantaneous ionic concentrations. We varied the magnitudes and durations of the conductance changes and the spine neck dimensions. We also compared the effectiveness of inhibition on the spine with inhibitory input on the dendrite at the base of the spine. The standard parameters used and details of the simulations are summarized in the caption of Fig. 1; any variation will be explicitly mentioned.

A measure of the effectiveness of shunting inhibition is the ratio of the maximum depolarization at a reference point in the neuron caused by an excitatory input alone to the depolarization when both the excitatory and the inhibitory inputs are present. This ratio, called the *F factor* (Koch and Poggio, 1983a), is equal to 1 if the inhibition has no effect on the excitation. One obvious requirement for effective inhibition is that its time course should overlap substantially with the excitatory synaptic conductance change. We modeled a spine located in the middle of a 300 μm-long dendrites and the response at the spine head was used to calculate F factors. Our simulation results based on both the cable model and the electro-diffusion model are shown in Table I. The cable model indeed showed strong veto effects, especially when the conductances were large, as predicted. However, our electro-diffusion model showed no significant veto effect over a wide range of conductances. Note also that when the $G_{Cl,M}/G_{Na,M}$ ratio was increased, there were cases where the F factor decreased slightly. This occurred because the Cl^- Nernst potential shifted so much that it depolarized the membrane away from its resting level. A Cl^- conductance change alone, however, did not cause any depolarization because there was no driving force and, therefore, no concentration change.

TABLE I. F Factors at the Spine Head when Both Excitatory and Cl^- Mediated Inhibitory Synaptic Inputs are Located on the Same Spine Predicted by Both the Electro-Diffusion Model and the Cable Model.

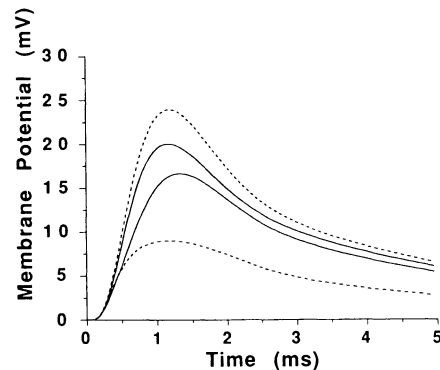| $G_{Cl,M}/G_{Na,M}$	$G_{Na,M}$ = 0.1 nS		$G_{Na,M}$ = 1.0 nS		$G_{Na,M}$ = 10 nS	
	diffusion	cable	diffusion	cable	diffusion	cable
1	1.02	1.02	1.10	1.17	1.23	1.65
10	1.10	1.20	1.20	2.74	1.26	7.56
10^2	1.16	3.04	1.19	18.63	1.25	66.20
10^3	1.14	20.35	1.19	163.86	1.25	602.19

FIGURE 2.   Postsynaptic responses relative to the resting level at the spine head calculated with the electro-diffusion model (solid lines) and the cable model (dotted lines). Two traces are shown for each model: The top trace is the response with excitatory synaptic input alone and the lower trace is the response to both excitatory and shunting inhibitory inputs. Excitatory synaptic input: $G_{Na,M} = 1$ nS; inhibitory synaptic input: $G_{Cl,M} = 10$ nS.

The difference between the cable model and the electro-diffusion model decreased as the synaptic conductances decreased. For $G_{Na,M} = 0.1$ nS, the two models were essentially identical and both predicted that the inhibition was ineffective. However, for longer durations of the synaptic input, the two models may not agree even for synaptic conductance changes as small as 0.1 nS. (See Section VI.) The details of the postsynaptic responses on the spine head are shown in Fig. 2.

Quantal analysis on excitatory postsynaptic potentials in area CA3 of the rat hippocampus (Higashima et al., 1986; Brown et al., 1988) gave a quantal conductance of about 1 nS at mossy fiber synapses. Therefore, the synaptic conductance change due to a single presynaptic action potential should be about a few nS. Similar measurements of unitary inhibitory conductance performed on CA3 pyramidal cells of guinea-pig hippocampus obtained a value of 5–9 nS (Miles and Wong, 1984). However, the conductance of synapses on pyramidal cells in cerebral cortex may be much smaller. In the following simulations, we fixed $G_{Na,M}$ at 1 nS and varied $G_{Cl,M}$ unless otherwise indicated.

The morphologies of spines vary greatly. The critical parameters for our simulations were the diameter and length of spine neck, which were varied from 0.1 µm to 0.25 µm and 0.4 µm to 1.0 µm, respectively, with the neck membrane area kept constant. We also considered the case where there was no spine neck and the spine head was connected directly to dendrite. The cable model gave large F factors when the neck was long and narrow and/or $G_{Cl,M}$ was large, but

the electro-diffusion model produced no F factor larger than 2 over the entire range. The effectiveness of inhibition was not very sensitive to the dimensions of the spine neck because of two competing effects that cancel: As the spine neck length was decreased and the diameter increased, the concentration changes in the spine were reduced, making the inhibition more effective. However, the input resistance of the spine head was also decreased, resulting in a smaller depolarization and a reduced driving force for the inhibition.

1. On-Path Inhibition.   Inhibitory synapses on pyramidal neurons are commonly located on the dendritic shaft at the base of the spine (Beaulieu and colonnier, 1985; Martin, 1984). The simulations in Fig. 3 show that dendritic on-path inhibition is much more effective than inhibition on the spine head. The ionic concentration changes were much smaller for the dendritic inhibition because the dendrite had a diameter of 1 μm, and hence the cable equation was a good approximation. Also, the driving force for the inhibition was strong because the spine was electrically coupled to the dendrite well enough that the excitation of the spine caused a large depolarization at the dendritic shaft.

2. Duration of Inhibition.   Table II shows the F factors at the spine for a range of durations of the synaptic conductance (determined by t_{peak} in Fig. 1). A longer duration produced a larger membrane depolarization that increased the driving force for the inhibition and made the inhibition more effective. This
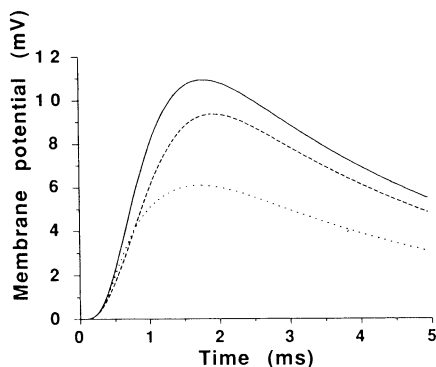

FIGURE 3.   Responses relative to the resting level at the dendritic shaft at the base of a spine under three conditions: no inhibition and the excitatory input ($G_{Na,M} = 1$ nS) on the spine head alone (solid), the excitatory input ($G_{Na,M} = 1$ nS) and the inhibitory input ($G_{Cl,M} = 10$ nS) both on the same spine head (dashed), and the excitatory input ($G_{Na,M} = 1$ nS) on the spine head and the inhibitory input ($G_{Cl,M} = 10$ nS) on the dendritic shaft at the base of the spine (dotted).

TABLE II. F Factors at the Spine for a Range of
Durations of the Synaptic Conductance. The time
to peak (t_{peak}, explained in caption to Fig. 1a) was
varied for a synapse with $G_{Na,M} = 1$ nS and $G_{Cl,M}$
$= 11$ nS.

t_{peak}(ms)	diffusion	cable
0.5	1.32	2.46
1.0	1.20	2.73
2.0	1.17	3.01
3.0	1.16	3.30
4.0	1.17	3.53

explains the increase of F factors with t_{peak} predicted by the cable model. However, the longer the conductance change, the larger the concentration change, which makes inhibition less effective according to the electro-diffusion model. The latter factor predominated for inhibition on the spine head, as shown in Table II.

Repetitive stimulation of inhibitory interneurons in hippocampal slices for tens of seconds can cause disinhibition of inhibitory potentials in pyramidal cells (Thompson and Gahwiler, 1989). The most likely explanation is the intracellular accumulation of Cl^-. Our simulations suggest that a similar disinhibition can occur on spines within milliseconds. The difference between the time scales can be attributed to the difference between the intracellular volumes of cell bodies and dendrites compared with spine heads.

3.   Interactions between Synapses on Dendrites.   We next studied interactions between excitatory and inhibitory synapses at adjacent sites on dendrites ranging in diameter from 0.1 to 2.0 μm. The predicted F factors for the cable model, given in Table III, were very large when the dendritic diameter was small and the G_{Cl} was large. For the electro-diffusion model, two competing factors determined the effectiveness of inhibition: For dendrites with large diameters, the concentration effects were small, so the Nernst potential did not change very much and the inhibition was effective. However, the polarization of the membrane from the resting level was smaller in larger dendrites, which made inhibition less effective. The F factors in Table IIIa were not monotonically increasing with increasing dendritic diameter because of these two factors and their interaction. For $G_i = G_e$, the first factor dominated and the inhibition was comparatively more effective on small dendrites. When $G_i \geq 100 \, G_e$, the second factor dominated and the inhibition was more effective on large dendrites. In any case,

TABLE III. F Factors for Both Excitatory and Inhibitory Synapses on Dendrites at the Same Site, with Different Dendritic Diameters. $G_{Na,M} = 1$ nS. Top: Electro-Diffusion Model; Bottom: Cable Model.

$G_{Cl,M}/G_{Na,M}$	dendritic diameter (μm)				
	0.1	0.25	0.5	1.0	2.0
0.1	1.07	1.04	1.02	1.01	1.00
1	1.47	1.45	1.18	1.07	1.03
10	1.87	1.66	2.26	1.66	1.31
10^2	1.91	2.67	3.43	3.10	3.25

$G_{Cl,M}/G_{Na,M}$	dendritic diameter (μm)				
	0.1	0.25	0.5	1.0	2.0
0.1	1.08	1.06	1.04	1.02	1.01
1	1.72	1.39	1.19	1.08	1.04
10	8.31	5.16	3.03	1.88	1.38
10^2	73.07	43.15	22.46	11.01	5.65

when the dendritic diameter was 0.1 μm, the F factors were always less than 2, similar to the previous results for inhibition on spines.

4. K^+-Mediated Inhibition.   The equilibrium potential for K^+ is generally below the resting membrane potential (12 mV below in our model), so that an increase in K^+ conductance leads to a hyperpolarization. In a previous study, we found that inhibition on spines mediated by K^+ was not effective for excitatory conductances greater than 10 nS (Qian and Sejnowski, 1989). In this section, we consider excitatory conductances that are lower and more realistic for pyramidal neurons. We find that for smaller excitatory conductances, hyperpolarizing inhibition can be quite effective. Synaptic responses to $G_{Na,M} = 0.1$ nS are shown in Fig. 4, which also shows that an inhibition of $G_{K,M} = 1$ nS is very effective in reducing the response. In comparison, the inhibition due to a similar or much larger conductance change for Cl^- was not effective. For large excitatory conductance changes, the K^+ inhibition became as ineffective as Cl^- because of the large K^+ concentration changes that rapidly shift the K^+ Nernst potential, as shown in Table IV.

Inhibition mediated by K^+ in cortical neurons has a time course that can last for a significant fraction of a second when it is activated by $GABA_B$ receptors
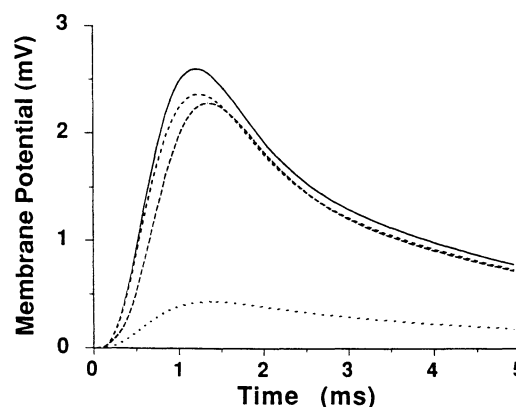
FIGURE 4.   Response relative to the resting level at the spine head to an excitatory input of $G_{Na,M} = 0.1$ nS and one of the following four different inhibitory synaptic inputs: no inhibition (solid), K^+ inhibitory synaptic input with $G_{K,M} = 1$ nS (dotted), Cl^- inhibitory input with $G_{Cl,M} = 1$ nS (dashed), and $G_{Cl,M} = 100$ nS (long-dashed).

through G proteins. We therefore studied the steady-state behavior following a step change in conductances of $G_{Na} = 0.1$ nS and $G_K = 1$ nS and found that the response at the spine head was about 6.9 mV with excitation alone and 1.3 mV with both excitation and inhibition. In steady state, the K^+ efflux from the spine head was balanced by the K^+ diffusion from the dendritic shaft to the head. Thus, the inhibition mediated by K^+ conductances remained effective for slow inhibitory synaptic potentials when the excitatory conductances were small. Since an excitatory synaptic conductance typically lasts for only a few ms, an excitatory input arriving a few ms earlier than the inhibitory input will not be affected by the inhibition. Once an inhibitory input is active, there is a long time window during which arriving excitatory inputs are inhibited.

TABLE IV. F Factors at the Spine Head when Both Excitatory and K^+ Mediated Inhibitory Synaptic Inputs are Located on the Same Spine Predicted by both the Electro-Diffusion and the Cable Models.

$G_{K,M}/G_{Na,M}$	$G_{Na,M} = 0.1$ nS		$G_{Na,M} = 1.0$ nS		$G_{Na,M} = 10$ nS	
	diffusion	cable	diffusion	cable	diffusion	cable
0.1	1.01	1.07	1.02	1.07	1.07	1.07
1	1.11	1.18	1.24	1.33	1.58	1.79
10	6.05	8.03	7.35	17.65	1.70	47.53
10^2	*	*	*	*	1.66	*

*F factors undefined because the responses were hyperpolarizing, indicating very effective inhibition.

V. The Cable Model for Electro-Diffusion

The electro-diffusion model is highly computation-intensive and cannot be used routinely for large-scale simulations of complex dendritic trees (Wathey *et al.* 1989). It would be desirable to have a model that was as efficient as the cable model. We will prove here that a simple extension of the cable model can, in fact, provide an accurate approximation to the predictions of the electro-diffusion model.

The following modifications to the discrete approximation of the standard cable model should be made at each time step:

(1) Calculate the intracellular concentration of each ionic species explicitly in each compartment from the membrane currents and the ionic currents flowing between compartments.

(2) Compute the new membrane equilibrium potentials for each compartment using the intracellular and extracellular ionic concentrations according to the Nernst equation and update the membrane batteries:

$$E_k = \frac{RT}{Fz_k} \ln \frac{n_k(\text{out})}{n_k(\text{in})}, \tag{17}$$

where $n_k(\text{out})$ is the ionic concentration of species k outside the membrane and $n_k(\text{in})$ is the ionic concentration inside the membrane. This makes the membrane current expressions identical to those used in the electro-diffusion model.

(3) Replace the single longitudinal resistance between compartments with parallel resistances $R_{i,k}$ (Qian and Sejnowski, 1989).

$$\frac{1}{R_{i,k}} = (F^2/RT)D_k n_k z_k^2, \tag{18}$$

in series with batteries (step 4) for each ionic species.

(4) Determine the longitudinal batteries by the Nernst potential for ionic concentrations of the two compartments they connect and update in the same way as the membrane batteries. The potential of the battery for species k between compartments j and $j + 1$ is:

$$E_{i,k} = \frac{RT}{Fz_k} \ln \frac{n_k(j)}{n_k(j + 1)}, \tag{19}$$

where a positive value for $E_{i,k}$ means that the positive terminal of the battery is pointing to the $j + 1$ compartment.

Steps 3 and 4 account for the effects of the longitudinal component of electrodiffusion in Eq. (11). We show here that this approximation is exact in limit that the compartments approach zero length.

Consider two compartments at x and $x + dx$. The longitudinal battery for ionic species k between these two compartments, according to step 4, is:

$$dE_{i,k}(x) = \frac{RT}{Fz_k} \ln\frac{n_k(x)}{n_k(x + dx)} = -\frac{RT}{Fz_k} \ln\left[1 + \frac{1}{n_k}\frac{dn_k}{dx}dx \right] = -\frac{RT}{Fz_k}\frac{dn_k}{n_k}\frac{dn_k}{dx}dx.$$

For a nerve fiber of cross-sectional area A, the ionic current of species k between these two compartments is:

$$I_k(x) = \frac{dE_{i,k}(x) + V(x) - V(x + dx)}{R_{i,k}dx/A}$$

$$= -AFz_kD_k\frac{dn_k}{dx} - \frac{AFz_kD_kn_k}{\alpha_k}\frac{dV}{dx}. \quad (20)$$

Equation (18) and the definition of α_k in Eq. (12) were used in this derivation. The flux $J_k(x)$ is defined as the number of ions moving across a unit area in unit time, of ionic species k between the two compartments. Thus, from Eq. (20),

$$J_k(x) = \frac{I_k(x)}{AFz_k} = -D_k\left[\frac{dn_k}{dx} + \frac{n_k}{\alpha_k}\frac{dV}{dx}\right], \quad (21)$$
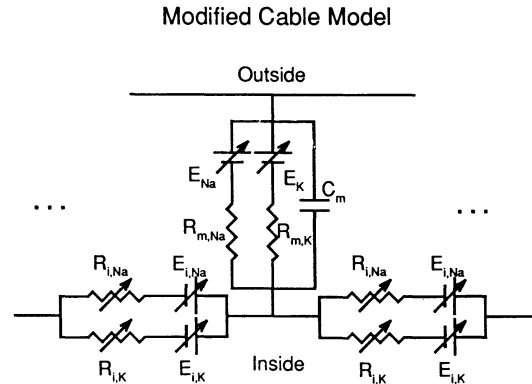
Modified Cable Model

FIGURE 5.   Electrical circuit for a single compartment of the modified cable model. The batteries in the membrane and between compartments are calculated from the Nernst potentials and change value during a response as concentrations change. The resistivities in the cytoplasm are also updated at each time step.

which is identical to the longitudinal component of the Nemst–Planck electro-diffusion equation for ionic species k. The continuity equation of the electro-diffusion model (Eq. (13)) is also satisfied in cable model because of Kirchoff's law. Therefore, results predicted by the modified cable model should be equivalent to those of the one-dimensional electro-diffusion model.

A schematic view of the modified cable model is represented in Fig. 5. This model was applied to the dendritic spine model in Qian and Sejnowski (1989). The results were in excellent agreement with the electro-diffusion model except when the conductances and ionic concentrations changed very rapidly. The differences were mainly due to the fact that we used the constant-field approximation for the membrane currents in that version of the electro-diffusion model, but used ohm's law for the batteries in the modified cable model.

VI. Discussion

In most circumstances, the cable model of electrical conduction in neurons gives accurate predictions for membrane potentials during transient electrical events. A tiny amount of charge is enough to cause a substantial change in the membrane potential because the membrane capacitance is small, and as a consequence, the ionic concentrations usually are nearly constant (Qian and Sejnowski, 1989). However, the *individual* concentrations of certain ions could change significantly as long as changes in the total charge are nearly balanced out. This is more likely to happen in very small structures such as dendritic spines and for an ion such as Ca^{++}, which is normally maintained at a very low concentration inside a cell. Thus, the predictions from the cable model should not be used without a careful analysis.

We have developed a one-dimensional electro-diffusion model of electrical conduction, which reduces to the cable model when ionic concentrations are approximately constant. This model was used to study changes in ion concentrations and membrane potentials in dendritic spines in response to synaptic inputs. We found that ionic concentrations changed considerably in many circumstances. Thus, significant errors can be made in estimating membrane potentials and concentration changes using the cable model if the effects of diffusion and the changes in the driving forces for membrane current are not taken into account.

The major conclusion of this study is that Cl^- shunting inhibition on spines cannot be very effective regardless of how large the synaptic conductance changes are. Shunting inhibition is significantly more effective when it is on the dendritic shaft on-path to the cell body. This may partly explain the anatomical findings

that most synapses on spines are putatively excitatory and that the majority of the putative inhibitory synapses are found on dendritic shafts. Shunting inhibitory synapses on spines may have other functions. Although they may not contribute significantly to the electrical responses of the cell, they can certainly cause large local ionic concentration changes that may be important in regulating certain cellular functions.

The inhibitory synapses on spines may contribute to the electrical responsiveness of a cell if they are mediated through K^+ currents. Our simulations predict that K^+ hyperpolarizing inhibition on a spine head can be very effective when the excitatory synaptic conductance changes are less than 10 nS. The major inhibitory neurotransmitter in the visual cortex is GABA; $GABA_A$ receptors are coupled to Cl^- channels and $GABA_B$ receptors are linked to K^+ channels. Therefore, we specifically predict that the inhibition on spines is mediated by the $GABA_B$ receptors. This prediction is consistent with the finding that $GABA_B$ input to hippocampal pyramidal cells is preferentially dendritic (Janigro and Schwartzkroin, 1988), where the majority of inputs are onto spines. Another way to have effective inhibition on a spine is through conductance decreases of either Na^+ or Ca^{++}, although this type of inhibitory mechanism has not been found in cortical neurons.

All these results can be understood as a consequence of changing ionic concentrations and shifting equilibrium potentials. The postsynaptic responses are mainly determined by the ionic species with the largest transient membrane permeability. Regardless of the equilibrium potential for this species (excitatory or inhibitory), the opening of channels with sufficient duration will shift the equilibrium potential of the synapse toward zero because of the large concentration changes. Therefore, if the equilibrium potential of the ionic species is greater than zero (Na^+ and Ca^{++}), the cable model will overestimate the response. For ions whose equilibrium potential is less than zero (K^+ and Cl^-), the cable model makes predictions that can be qualitatively incorrect. For example, under certain conditions an inhibitory synaptic input that causes a large K^+ conductance increase may, in fact, produce a postsynaptic depolarization.

Our simulations have shown that discrepancies between the cable model and our electro-diffusion model increase with the magnitude and duration of the synaptic conductance changes. Since the cable model is valid only when the concentration changes are small, we can derive a condition under which the cable model is self-consistent. The intracellular concentration change of the kth ionic species caused by membrane current I_k within time duration Δt is $\Delta n_k = I_k \Delta t / vzF$, where v is the effective intracellular volume, z is the valence of the ion involved, and F is the Faraday's constant. (Of course, n_k will eventually stop changing with time when the membrane current is balanced by the intra-

cellular diffusion.) The criteria for the self-consistency of the cable model is simply $|\Delta n_k|/n_{k,0} \ll 1$, where $n_{k,0}$ is the initial intracellular ionic concentration, or $\Delta t \ll |vzFn_{k,0}/I_k|$.

When the synaptic conductance G_k is small, say, 0.1 nS, $I_k \sim G_k E_k$, where E_k is the reversal potential relative to the resting potential. The preceding condition gives $\Delta t \ll 10$ ms for Na^+ in a spine, assuming that the effective volume v is equal to twice the volume of the spine. Therefore, the cable model may not be valid for spines if the duration of the conductance change is longer than 10 ms, even for synaptic conductance changes as small as 0.1 nS. the inclusion of ionic pumps would not alter the preceding conclusions for a typical Na–K pump current density of $1 \sim \mu A/cm^2$ (Weer and Rakowski, 1984), in which case the total pump current of the spine head is about 10^{-14} A, three orders of magnitude smaller than the synaptic current. Even when the pump molecules are close-packed in the membrane, the maximum possible pump current density is 100 $\mu A/cm^2$, and the total pump current of the spine head is still about 10 times smaller than the synaptic current for a 0.1 nS conductance. The effect of the Na–K pump would be significant if we assume that the spine apparatus is also densely packed with pump molecules and its surface area is about 10 times that of the spine.

Ionic concentration changes are usually not explicitly considered in the cable model. Although ionic currents in the cable model can be integrated to yield concentration changes, this usually gives erroneous results (Qian and Sejnowski, 1989), even when the membrane potentials are predicted fairly well. Often, the cable model is solved first to find the membrane potentials and then diffusion processes are introduced to determine the ionic concentration changes (Gamble and Koch, 1987; Yamada *et al.*, 1989). Our model, however, considers the membrane potential and the ionic concentration changes at the same time and thus provides a more natural and accurate way for solving the problem.

In our simulations, we have assumed that extracellular ionic concentrations were constant to simplify our calculations. This may not be a valid approximation in restricted extracellular spaces for the same reasons that the cable model broke down in restricted intracellular spaces. If the extracellular space around a spine head that is effectively available for exchange in 0.5 ms is about the same as the volume of spine, then a change of concentration in the spine head would cause an equal change with opposite sign outside the spine head. For $t_p = 0.25$ ms, the extracellular $[Na^+]$ would change from 140 mM to about 110 mM, and $[K^+]$ from 4 mM to about 34 mM in about 0.5 ms. (See Yamada *et al.*, 1989 for a similar estimate.) Although the extracellular K^+ concentration would increase by a larger factor, the maximum value of an excitatory synaptic response

is mainly determined by the Nernst potential of Na^+ because the Na^+ permeability is much larger during an excitatory synaptic input. Also, glial cells are very effective in maintaining K^+ homeostasis on a longer time scale so that the actual change during maintained activity is probably less.

Thus, the main effect of a limited extracellular space is on the Nernst potential of Na^+. Based on the preceding estimates, this would reduce the peak response of the postsynaptic potential by about 6% at the spine head. For large t_p and multiple synaptic inputs, the Na^+ concentration change is greater but is achieved over a longer period of time. The corresponding effective extracellular space around the spine head would then be larger because more time allows ions to diffuse further. Thus, the modification would not be much greater. For an excitatory input driven by a Na^+ current, the effects of restricted extracellular space always reduce the amplitude of response and thus will tend to make the differences with the cable model even greater.

For synapses on large dendrites rather than on spines, we do not expect any significant difference between the electro-diffusion model and the cable model because the ionic concentration changes are negligible. Synaptic inputs on thick dendrites should not suffer the saturation caused by shifts of the Nernst potential, the absence of temporal summation, and lack of an inhibitory veto effect that we have demonstrated for synapses on spines. On the other hand, large compartments are also harder to depolarize, which is needed to increase the driving force of the inhibitory currents. This second factor may not be as important if a compartment also receives a large number of convergent excitatory synapses. Note that the more depolarized a cell, the more effective the inhibitory synapses become and the less effective the excitatory synapses. Indeed, if the depolarization is large enough to trigger an action potential, the driving forces for the inhibitory currents on soma and dendrites reach their maximum and the driving forces for the excitatory currents reach their minimum, especially if the effects of the action potentials propagate up the dendritic tree. Thus, inhibitory synapses on the cell body and proximal dendrites could control the effects of action potentials propagating up dendritic trees and the temporal firing patterns of the neuron (Lytton and Sejnowski, 1991).

This raises the interesting possibility that otherwise identical synapses could have different functions depending on their location. It has been reported that during learning and development, the spine neck shortens and merges into the dendrite (Rausch and Scheich, 1982; Coss and Globus, 1978; Brandon and Coss, 1982; Coss *et al.*, 1980). The concentration changes in spines are caused not just by the small volume of the spine head but also by the long, narrow spine neck, which helps to maintain the large concentration changes that occur in the spine head. Thus, synapses on spines with long necks could switch to a different

functional state if the neck were to shorten sufficiently for the spine to merge with the dendritic shaft.

Acknowledgments

References

BEAULIEU, C., and COLONNIER, M. (1985). "A Laminar Analysis of the Number of Round-Asymmetrical and Flat-Symmetrical Synapses on Spines, Dendritic Trunks, and Cell Bodies in Area 17 of the Cat," *J. Comp. Neuro.* **231,** 180–189.

BRANDON, J. G., and COSS, R. G. (1982). "Rapid Dendritic Spine Stem Shortening during One-Trial Learning: the Honeybee's First Orientation Flight," *Brain Research* **252,** 51–61.

BROWN, T., CHANG, V., GANONG, A., KEENAN, C., and KELSO, S. (1988). In P. Landfield and S. Deadwyler (eds.) *Long-Term Potentiation: From Biophysics to Behavior* (pp. 201–264). Alan R. Liss, New York.

COSS, R. G., BRANDON, J. G., and GLOBUS, A. (1980). "Changes of Morphology of Dendritic Spines on Honeybee Calycal Interneurons Associated with Cumulative Nursing and Foraging Experiences," *Brain Research* **192,** 49–59.

COSS, R. G., and GLOBUS, A. (1978). "Spine Stems on Tectal Interneurons in Jewelfish Are Shortened by Social Stimulation," *Science* **200,** 787–789.

COSS, R. G., and PERKEL, D. H. (1985). "The Function of Dendritic Spines," *Behavioral and Neural Biology* **44,** 151–185.

GAMBLE, E., and KOCH, C. (1987). "The Dynamics of Free Calcium in Dendritic Spines in Response to Repetitive Synaptic Input," *Science* **236,** 1311–1315.

GRIFFITH, W., BROWN, T., and JOHNSTON, D. (1986). "Voltage-Clamp Analysis of Synaptic Inhibition during Long-Term Potentiation in Hippocampus," *J. Neurophysiol.* **55,** 767–775.

HARRIS, K. M., and STEVENS, J. K. (1989). "Dendritic Spines of CA1 Pyramidal Cells in the Rat Hippocampus: Serial Electron Microscopy with Reference to Their Biophysical Characteristics," *J. Neurosci.* **9,** 2982–2997.

HIGASHIMA, M., SAWADA, S., and YAMAMOTO, C. (1986). "A Revised Method for Generation of Unitary Postsynaptic Potentials for Quantal Analysis in the Hippocampus," *Neuroscience Letter* **68,** 221–226.

HILLE, B. (1984). *Ionic Channels of Excitable Membranes.* Sinauer Associates, Sunderland, Massachusetts.

HODGKIN, A. L., and HUXLEY, A. F. (1952). "Currents Carried by Sodium and Potassium Ions through the Membrane of the Giant Axon of *Loligo*," *J. Physiol.* **116,** 449–472.

HUGUENARD, J., and ALGER, B. (1986). "Whole-Cell Voltage-Clamp Study of the Fading of the GABA-Activated Currents in Acutely Dissociated Hippocampal Neurons," *J. Neurophysiol.* **56,** 1–18.

JACK, J. J. B., NOBLE, D., and TSIEN, R. W. (1975). *Electrical Current Flow in Excitable Cells*. Oxford University Press, Oxford.

JANIGRO, D., and SCHWARTZKROIN, P. (1988). "Effects of GABA on CA3 Pyramidal Cell Dendrites in Rabbit Hippocampal Slices," *Brain Research* **453**, 265–274.

KOCH, C., POGGIO, T., and TORRE, V. (1982). "Retinal Ganglion Cells: A Functional Interpretation of Dendritic Morphology," *Phil. Trans. R. Soc. Lond.* **298**, 227–264.

KOCH, C., and POGGIO, T. (1983a). "A Theoretical Analysis of Electrical Properties of Spines," *Proc. Roy. Soc. Lond.* **B218**, 455 –477.

KOCH, C., and POGGIO, T. (1983b). "Electrical Properties of Dendritic Spines," *Trends in Neuroscience* **3**, 80–83.

KOCH, C., POGGIO, T., and TORRE, V. (1983). "Nonlinear Interaction in a Dendritic Tree: Location, Timing, and Role in Information Processing," *Proc. Natl. Acad. Sci. USA* **80**, 2799–2802.

LYTTON, W. W., and SEJNOWSKI, T. J. (1991). "Simulations of Cortical Pyramidal Neurons Synchronized by Inhibitory Interneurons." *J. Neurophys.* **66**, 1059–1079.

MARTIN, L. F. (1984). "Morphology of the Neocortical Pyramidal Neurons," A. Peters and E. G. Jones (eds.), *Cerebral Cortex, Vol. 1* (pp. 123–200). Plenum, New York.

MILES, R., and WONG, R. (1984). "Unitary Inhibitory Synaptic Potentials in the Guinea-Pig Hippocampus *in vitro*," *J. Physiol.* **356**, 97–113.

PERKEL, D. H., and PERKEL, D. J. (1985). "Dendritic Spines: Role of Active Membrane Modulating Synaptic Efficacy," *Brain Research* **325**, 331–335.

QIAN, N. and SEJNOWSKI, T. J. (1988). "Electro-Diffusion Model of Electrical Conduction in Neuronal Processes," in C. W. Woody, D. L. Alkon, and J. L. McGaugh (eds.), *Cellular Mechanisms of Conditioning and Behavioral Plasticity*. Plenum, New York.

QIAN, N. and SEJNOWSKI, T. J. (1989). "An Electro-Diffusion Model for Computing Membrane Potentials and Ionic Concentrations in Branching Dendrites, Spines and Axons," *Biol. Cybernetics* **62**, 1–15.

QIAN, N. and SEJNOWSKI, T. J. (1990). "When is an Inhibitory Synapse Effective?" *Proc. Natl. Acad. Sci USA* **87**, 8145–8149.

RALL, W. (1977). "Core Conductor Theory and Cable Properties of Neurons," in E. R. Kandel (ed.), *Handbook of Physiology: The Nervous System:* (pp. 39–97). American Physiological Society, Bethesda, Maryland.

RALL, W. (1978). "Dendritic Spines and Synaptic Potency." in R. Porter (ed.), *Studies in Neurophysiology*. Cambridge University Press, Cambridge.

RALL, W., and SEGEV, I. (1987). "Functional Possibilities for Synapses on Dendrites and Dendritic Spines," in G. M. Edeleman, W. F. Gall, and W. M. Cowan (eds.), *New Insights into Synaptic Function*. John Wiley, New York.

RAUSCH, G., and SCHEICH, H. (1982). "Dendrite Spine Loss and Enlargement during Maturation of the Speech Control System in Mynah Bird *Gracula religiosa*," *Neurosci. Lett.* **29**, 129–133.

SHEPHERD, G. M., BRAYTON, R. K., MILLER, J. P., SEGEV, I., and RALL, W.

(1985). "Signal Enhancement in Distal Cortical Dendrites by Means of Interactions between Active Dendritic Spines," *Proc. Natl. Acad. Sci. USA* **82,** 2192–2195.

THOMPSON, S. M., and GAHWILER, B. H. (1989). "Activity-Dependent Disinhibition, I. Repetitive Stimulation Reduces IPSP Driving Force and Conductance in the Hippocampus *in vitro*," *J. Neurophysiol.* **61, 501–511.**

WATHEY, J., LYTTON, W., JESTER, J., and SEJNOWSKI, T. (1989). "Simulations of Synaptic Potentials Using Realistic Models of Hippocampal Pyramidal Neurons," *Soc. Neuroscience Abstracts* **15.**

WEER, P. D., and RAKOWSKI, R. F. (1984). "Current Generated by Backward-Running Electrogenic Na$^+$ Pump in Squid Giant Axons," *Nature* **309,** 450–452.

YAMADA, W. M., KOCH, C., and ADAMS, P. R. (1989). "Multiple Channels and Calcium Dynamics," in C. Koch and I. Segev (eds.), *Methods in Neuronal Modeling.* MIT Press, Cambridge, Massachusetts.

ZADOR, A., KOCH, C., and BROWN, T. H. (1990). "Biophysical Model of a Hebbian Synapse," *Proceedings of the National Academy of Sciences USA* **87,** 6718–22.